



Catalytic hydrocracking of vegetable oil for agrofuels production using Ni–Mo, Ni–W, Pt and TFA catalysts supported on SBA-15

A.E. Barrón C.^a, J.A. Melo-Banda^{a,*}, J.M. Dominguez E.^b, E. Hernández M.^a, R. Silva R.^a, A.I. Reyes T.^a, M.A. Meraz M.^c

^a Instituto Tecnológico de Ciudad Madero, División de Estudios de Posgrado e Investigación, Juventino Rosas y Jesús Urueta S/N, C. P. 89440, Col. Los Mangos, Cd. Madero, Tamaulipas, Mexico

^b Instituto Mexicano del Petróleo, Programa de Ingeniería Molecular, Eje central L. Cárdenas No. 152, Col. San Bartolo Atepehucan, Del. Gustavo A. Madero, México, D.F., Mexico

^c Instituto Tecnológico de Iztapalapa-III, Av. Cuitlahuac, Col. Los Reyes Culhuacan, Del. Iztapalapa, México, D.F., Mexico

ARTICLE INFO

Article history:

Available online 16 February 2011

Keywords:

Biofuels
Vegetable oil
Carbides
Platinum
Mesoporous materials
SBA-15
SBA-16

ABSTRACT

Forecasting studies based upon Hubbert's type multicyclic calculations indicate a progressive declining of most of the fossil oil sources worldwide after reaching a production maximum [1]. In the near future scenario the search of renewable alternate fuels sources will be of increasing importance, for example agrofuels, which are fuel grade derivatives of vegetable oils; thus, this work deals with newer catalysts for selective hydrocracking of long hydrocarbons chains derived from safflower oil, i.e., heterogeneous catalysts supported on mesoporous SBA-15 were prepared and tested for hydrocracking of the unsaturated oil. For this, a series of catalysts based upon Ni–Mo, Ni–W carbides, Pt and triflic acid were characterized by N₂ physisorption (BET), X-ray diffraction (XRD), transmission electron microscopy (TEM) and pyridine adsorption-DRIFTS. In parallel, their activity, selectivity and operation conditions were followed and the reaction products were analyzed by GC. The viscosity and API density of the liquid products thus obtained were classed as products equivalent to medium crude oil fractions. Naphtha (C₅–C₉) was produced with a total yield in the interval 15–30 wt.%, while light products represented less than 5 wt.%. Two outstanding catalysts based upon trifluoromethanesulfonic acid produced naphtha and light compounds with a yield higher than 30% and 15%, respectively, which indicates the strong influence of the surface acidic active sites on the cracking reactions of long chain hydrocarbons derived from vegetable oils.

© 2011 Elsevier B.V. All rights reserved.

1. Introduction

The progressive declining of oil production worldwide and stringent environmental issues have motivated an increasing interest and new scientific research on alternative fuels recently. Statistical calculations based upon Hubbert's model indicate that 23 of the bigger 44 fossil oil producers worldwide have overcome or are near to pass over their maximum production point [1]. On the other hand, more environmental concerns have enforced laws which point out the need of reducing or in some cases eliminate fuels emission contaminants such as SO_x, NO_x, aromatics and suspended particles, but global greenhouse gas (CO₂) emissions is becoming also of primary concern, as expressed recently in the Cancun summit [2]. In this scenario, it has been postulated that a better balance could be attained by the progressive substitution of "fossil fuels" by alternative fuels derived from green plants, which tend to be considered already as







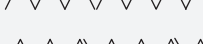
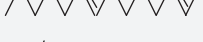


commodities and valuable options to complement or even replace those derived from petroleum [3]. In fact, commercial gasoline containing ethanol is offered as "ecological fuel" (i.e., E10: 10% ethanol–90% fossil fuel; E20: 20% ethanol–80% fossil fuel; and E30: 30% ethanol–70% fossil fuel). In this case ethanol is derived from sugar cane, beet or corn. This fuel comply regulations about the oxygen content of at least 2 vol.% and this seems to be more advantageous than methyl-ter-butyl ether (MTBE), a current gasoline additive that has been blamed to cause a negative environmental impact on soil and underground water. Furthermore, pure "agrofuels" are almost sulfur-free. The high content of lipids in most of vegetable oils arises from their fatty acid composition, either saturated or unsaturated (i.e., mono-and-poly-unsaturated). The saturated fatty acids are composed by hydrocarbons chains ranging from 4 (butyric acid) to 35 carbons (cero-plaste acids) and the most abundant ones have 14, 16 or 18 carbon atoms chains and are rather stable (i.e., low chemical reactivity). In contrast, the unsaturated fatty acids may have one to six double bonds along the chain and for this reason are more reactive with respect to the saturated ones. The most common structures of fatty acids are described in Table 1 with a nomenclature proposed in this work as follows: C18:2n-

* Corresponding author.

E-mail address: melobanda@yahoo.com.mx (J.A. Melo-Banda).

Table 1

Fatty acid compounds in natural products.

Structure	Nomenclature	Common name	Natural source
	C10:1 n-1	Capreol	Ruminants milk
	C12:1 n-3	Lauroleic	Cow milk
	C16:0	Palmitic	All fats
	C16:1 n-7	Palmitoleic	Nut and fish oil
	C 18:1 n-9	Oleic	Vegetable oil
	C18:1 n-7	Vaccenic	Ruminant fat
	C18:2 n-6	Linoleic	Vegetable oils (sunflower, corn, soy)
	C18:2 n-3	Linolenic	Soy and other vegetable oils
	C20:0	Arachidic	Peanut oil
	C20:1 n-11	Gadola	Fish oil

6, means a molecule with 18 carbons and 2 unsaturated bonds, which are located every 6 carbons). A wide revision of the topic was reported by Kubickova and Kubicka [4]; more specifically Ooi and Zakaria [5] studied the catalytic cracking of palm oil using alumina catalysts and mesoporous materials (MCM-41), which gave a yield superior to 43 vol.% gasoline in a batch type reactor. Also, Charusiri and Vitidsant [6] studied the hydrocracking of vegetable oils to produce liquid fuels using a catalyst based upon sulfated zirconium oxide, with a final conversion to gasoline of about 24%. In the present work we considered the effect of the support pore diameter on the catalytic hydrocracking of vegetable oils, which is not only an important factor to promote optimal dispersion of metals but also a means for increasing molecular diffusion through the pores system, where most of surface active sites are located [7]. It was pointed out elsewhere that the number of carbons in vegetable oil hydrocarbon chains and its structure depend mainly on the fatty acid content; for safflower oil the carboxylic acids C18 (70–83%) predominate, i.e., C18:2 (from 9 to 20%); in turn, these hydrocarbons chains have an adequate size for their use as feedstock for hydrocracking catalytic processes. Also, Egia et al. [8] investigated the properties of NiMo sulfides supported on zeolites HY for the hydroconversion of n-decane. They found a moderate pressure effect at 3 MPa during the reaction but the catalysts were deactivated in the first hour of reaction. Reyes et al. [9] found that NiMo carbides and Ni-W/alumina catalysts had better catalytic properties than some industrial catalysts based on NiMo/Al₂O₃, because the NiMo carbides presented higher hydrosulfurization and hydrogenation rates. Barbosa and Carlota [10] studied the hydrocracking of cumene in the presence and absence of quinoline using NiMo/AlMCM-41 catalysts, their results indicated that these catalysts are very resistant to poisoning by nitrogen and presented a high activity for hydrocracking. Also, Galiasso and Caprioli [11] studied the effects of Ni-Mo/Al₂O₃ catalyst deactivation in a fluidized bed type reactor for heavy residues hydrocracking and the study demonstrated the formation of a coke layer both inside and outside the catalyst particles, which increases in thickness with the increase of the reaction temperature; a further characterization of the catalyst particles indicated a coke layer formed on the outer particle surface, which consists mainly of pre-graphitic carbon. In turn, coke deposited inside the pores reduce the pore

structural ordering, thus decreasing the reaction rate and preventing the spreading out of liquid reactants, which tends to diminish both conversion and selectivity. Also, the hydrocracking of long-chain paraffins like n-decane was studied by Shuangqin and Juliette [12] using Ni-W sulfides supported on Al-SBA-15; this catalyst is more active and selective towards isomerization with respect to commercial catalysts based upon silica-alumina. Similarly, Yori et al. [13] compared the use of Ni and Pt as promoters of ZrO₂-SO₄ in hydroisomerization and hydrocracking of n-octane, where the addition of Ni decreases the acid activity but increased selectivity to isoparaffins. The contribution of platinum does not seem to change the selectivity but provided stability to the catalyst. Strausz and Thomas [14] showed that a superacid catalyst based on boron trifluoride in hydrofluoric acid (HBF₃) is highly effective for hydrocracking oil shale. Although most of the catalysts described above have interesting properties for promoting the hydrocracking reactions of long-chain paraffins, there are only few reports on the use of those catalysts for vegetable oils hydrocracking, which is of great interest for “agrofuels” production. That is the main contribution of this work and it contributes further to understand how the support porous structure effects the whole behavior of the active phases for hydrocracking of vegetable oils, i.e., the use of mesoporous materials like SBA-15 was introduced as a valid support for the safflower oil hydrocracking. Also, this paper describes the effects of NiMo and NiW carbides, platinum and trifluoromethane sulfonic acid supported on SBA-15, on the hydrocracking type reactions using vegetable oils feedstock.

2. Experimental

2.1. Synthesis of the support

Mesoporous SBA-15 support was prepared using general procedures reported recently [15,16], using a triblock co-polymer (Pluronic 123) composed by chains of poly(ethyleneoxide)-poly(propyleneoxide)-poly(ethyleneoxide) (EO₂₀PO₇₀EO₂₀), which is the structure directing agent, plus tetraethyl orthosilicate (TEOS) as the silica source. In a typical synthesis, 4 g of Pluronic P123 is dispersed in 150 ml of HCl solution (0.5 M). Finally, 9 g of TEOS are added to a homogeneous solution with strong stirring.

The mixtures were stirred at 318 K for 24 h. Then, the reaction mixture was submitted to hydrothermal treatment (aging) at 363 K for 24 h. The resulting solids were isolated by filtration, washed with deionized water and dried at 353 K for 12 h. The SBA-15 precursor was calcined in air at 823 K for 6 h, with a slow temperature increase. Three different types of catalysts were obtained by supporting different chemical species on the mesoporous SBA-15 support, first bimetallic Ni–Mo and Ni–W carbides (i.e., atomic ratio of 0.5), with and without phosphorus (i.e., 1.5 wt.%), second was triflic acid (TFA) impregnated in two different concentrations by means of two methods, finally platinum salts were used to impregnate the support material with concentrations of 0.5 and 1 wt.%.

2.2. Synthesis of Ni–Mo and Ni–W carbides

The metallic oxide precursors were obtained by means of the incipient wetness technique, using $\text{Ni}(\text{NO}_3)_2$ (Chemical Aldrich Co., 99.99%) and $(\text{NH}_4)_6\text{Mo}_7\text{O}_{24} \cdot 4\text{H}_2\text{O}$ (Chemical Aldrich Co., 99.5%) with an atomic ratio $\text{Ni}/(\text{Ni}+\text{M}^+)$ of 0.5 (2.8 Mo atoms/nm², i.e., $\text{M}^+ \sim 15\text{--}18\text{ wt.}\%$ ($\text{M}^+ = \text{Mo or W}$) and $\text{Ni} \sim 7\text{--}11\text{ wt.}\%$ loads, where the surface area of the former support, before the reduction treatments, was used to calculate the metal contents (according to a specific atomic ratio); both materials were successively incorporated using ethanol as a solvent; afterward, the materials were dried at 393 K overnight. Phosphorus was incorporated using the same route with $(\text{NH}_4)_2\text{HPO}_4$ (Chemical Aldrich Co., 99%) in order to obtain 1.5 wt.% P loads. Later, the solids were dried at 393 K; afterward, the final material was calcined at 723 K. These materials were treated with reducing agents such as an anhydrous combination of $\text{CH}_4/\text{H}_2 = 2/1$, which is related to procedures reported elsewhere [17,18]. After reduction, all the solids loaded with metals were passivated under a mixture of a diluted flow of oxygen (O_2 : 1 vol.%) and helium (He), because some of them presented pyrophoric properties.

2.3. Synthesis of Pt catalysts

The catalysts based upon Pt/SBA-15 were impregnated in situ by co-condensation during the synthesis of SBA-15, according to the procedure reported by Park et al. [19]. This consists in adding a solution of acetyl acetonate platinum (II) ($\text{Pt}[\text{C}_5\text{H}_7\text{O}_2]$, i.e., 2.97% (0.5 and 1 wt.%) and aging was followed during 30 min. Afterwards, tetraethylorthosilicate (TEOS) was used as the silica source and it was added drop wise. The mixture was kept under stirring for 24 h at $T = 327\text{ K}$. Finally, the mixture was aged at $T = 363\text{ K}$ during 24 h. Subsequently, the solid was filtered out and dried at 333–363 K. Finally, in order to remove the organic structuring agent the materials were calcined at 823 K in a dynamic air atmosphere for 6 h.

2.4. Synthesis of TFA supported catalysts

The mesoporous support SBA-15 was impregnated with triflic acid according to the method reported by Ramos [20]. First, the mesoporous support SBA-15 was suspended in a solvent (water or acetone) using ratios of 1.5 g/20 ml, then the mixtures were stirred for 1 h and 30 min, respectively. Later, trifluoromethane sulfonic acid (TFA, $\text{CF}_3\text{SO}_3\text{H}$) was added to each solution with vigorous stirring for 12 h. The acidification of silicate in each solvent was calculated for obtaining a final content of 11 TFA mmol/g SBA-15).

2.5. Characterization

The textural properties of the catalysts were characterized by N_2 physisorption (BET method) using a Quantachrome Autosorb-1

apparatus. The structural properties of those materials were determined by X-ray diffraction (XRD) using a Diffractometer BRUKER AXS D8 ADVANCE with a $\text{CuK}\alpha$ X-ray source. Transmission electron microscopy (TEM) images were collected on a FEI Tecnai G² 30 microscope operated at 300 kV.

2.6. Reaction tests

1 g of catalyst and 400 ml of safflower oil were placed in a batch type stainless steel reactor (2 L, volume) which was heated by electrical means. The reactor was pressurized with adding N_2 inert atmosphere. Once the reactor reached the reaction temperature, N_2 was vented and a new flow of $\text{H}_2\text{--N}_2$ was introduced (i.e., molar ratio of 20–80, 10 kg/cm² pressure). The gas samples were collected in a gas camera bullet while the liquid fluid was kept in a glass container for chromatographic analysis (GC). The analysis of the reaction products was made using a Varian gas chromatograph model 3400, fitted with a flame ionization detector (FID) and a SPBTM-5 capillary column of 30 m length, 0.53 mm internal diameter and 0.5 μm thickness of a stationary phase.

3. Results

3.1. X-ray diffraction

Fig. 1 shows the X-ray diffraction pattern of the mesoporous support SBA-15 after calcination at 823 K. The main peaks corresponding to (100), (110) and (200) planes fit the hexagonal symmetry $p6mm$. The more intense reflection due to (100) type planes is characteristic of periodic pore arrays of SBA-15; the (110) and (200) planes coincide with a hexagonal symmetry, which indicates the 2D periodic arrangement of pores. The basal spac-

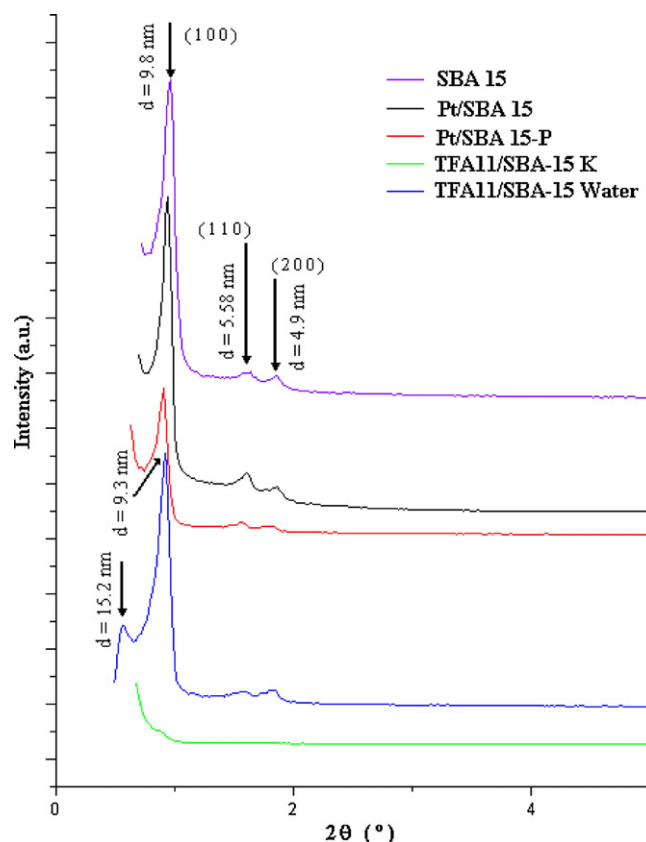


Fig. 1. X-ray diffraction patterns of support (SBA-15) and supported catalysts.

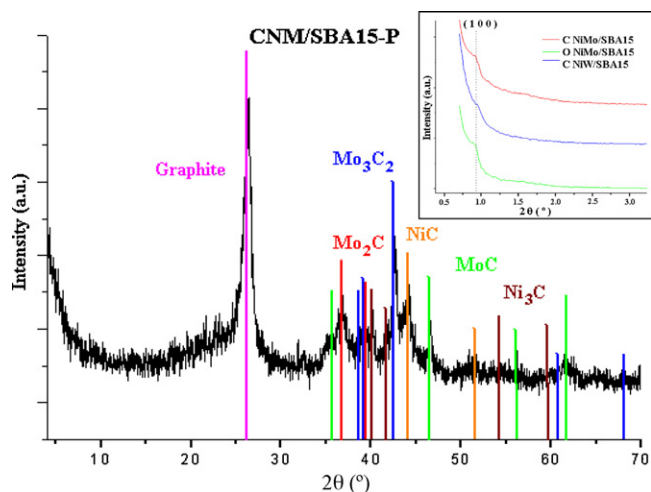


Fig. 2. X-ray diffraction pattern of the Ni–Mo carbide phases. Notice the typical graphitic component and separated (Mo,Ni)C phases.

ing is equal to 9.8 nm, which is typical of SBA-15. Similarly, the diffraction patterns of 1.0Pt/SBA-15 catalysts (with and without 1.5 wt.% phosphorus) are described in Fig. 1, where one observes that the three characteristic peaks of SBA-15 (i.e., approximately 0.86, 1.6 and 1.8° in 2θ scale) are not affected by the presence of platinum but the catalysts containing phosphorus (Pt/SBA-15-P) shows less intensity but still Pt/SBA-15 catalysts are stable and ordered materials. The contribution of Pt and P to the XRD pattern is very low at the concentration used in the Pt catalysts, especially because these elements are highly dispersed over the support surface. Also, Fig. 1 shows the X-ray diffraction pattern of the triflic acid impregnated catalysts, where one observes the permanence of the hexagonal porous arrangement after the acidic treatment with TFA aqueous solution, but the TFA in acetone solution (i.e., TFA11/SBA-15k) caused a destructive effect on the hexagonal pore arrays. In contrast, the peak appearing at or near to 9° in the 2θ scale for TFA11/SBA-15 Water catalyst indicates a preservation of the hexagonal pores array. However, these materials exhibit an extra peak at 0.58° (2θ), which is a broad and less intense peak, which could indicate the development of another pore system into the same catalyst; the new XRD peak has a basal spacing of 15.2 nm, which could be attributed to a second order or a pore system with diameters greater than the original pore diameter (i.e., 9.8 nm). The XRD pattern of TFA11/SBA-15-Water catalyst shows a weak peak at about 2° (2θ), this represents a shrinking decrease of about 0.5 nm of the basal spacing of the catalyst pores, with respect to the pure support. The XRD peaks of some catalysts (i.e., CNM and CNW) show a significant decrease of the hexagonal pore ordering after metals impregnation (Figs. 2 and 3). The XRD pattern of TFA11/SBA-15-Water shows a weak peak at about 2° (2θ), this represents a shrinking decrease of about 0.5 nm of the basal spacing of the catalyst pores, with respect to the pure support. This is attributed to the prevailing conditions during synthesis (i.e., near to 973 K), and high metal loads within the pores (i.e., approximately 15% Ni, 20% Mo and 30% W); metal and metal carbides might undergo at partial oxidation conditions that generate a heat release at a local level, within the catalyst pores, which may destroy the hexagonal pore symmetry and cause additional erosion to the pore system. Although the carburization process takes place at a temperature much higher than oxidation, the collapse of the hexagonal structure could occur during the formation of the metal oxides, because this reaction is exothermic and might release large heat bursts, which could provoke the collapse of the pore structure; in contrast, the carburization process is endothermic and occurs at high

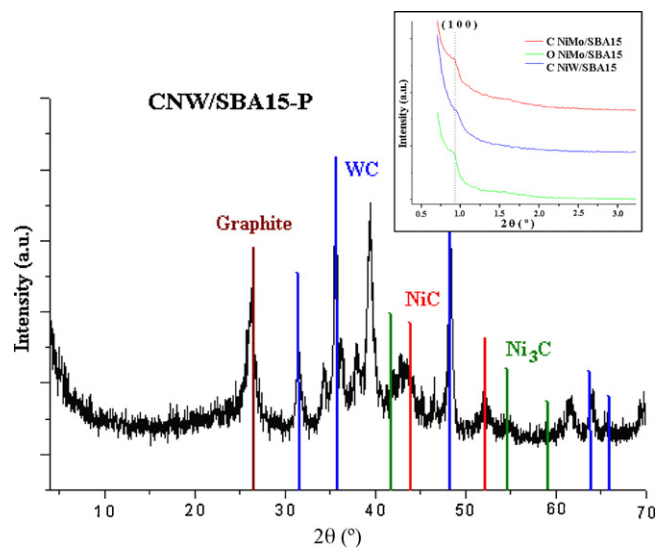


Fig. 3. X-ray diffraction pattern of the (Ni,W)C catalysts. Notice the peaks corresponding to (Ni,W) separated phases.

temperature, which could be enough to activate the reaction. This is confirmed even before the carburization of the catalyst by the appearance of a peak at 0.8° (2θ), which disappears during the formation process of Ni–Mo bimetallic oxides (Fig. 3). In the angular range 10–70° (2θ) there are some characteristic peaks corresponding to segregated phase carbides, i.e., MoC, Mo₃C₂, Mo₂C, NiC and Ni₃C, in the case of bimetallic carbides of Ni–Mo (Fig. 2), and compounds like NiC, Ni₃C WC carbides in the case of bimetallic carbides of Ni–W (Fig. 3). All the carbide type catalysts report the presence of graphitic material with an intense peak near to 26° (2θ), which is attributable to deposition of carbon during CH₄ dehydrogenation, whereas the presence of the phosphorus compounds was not detected by XRD due to its low concentration on the solids surface.

3.2. Morphological properties

The SBA-15 support was characterized by scanning electron microscopy (SEM). Fig. 4 shows the morphology of the mesoporous silicate particles as synthesized, where one observes clearly a number of individual particles and aggregates with hexagonal prismatic form of about 1 to 2 μ m length.

3.3. Structural properties

The transmission electron micrographs exhibit a fine structure in most of the catalytic materials. Fig. 5 illustrates the hexagonal pore arrays and pores have a diameter of about 4 nm and a wall thickness of 7 nm, approximately. Also, a side view of the particle is observed with a spacing between lamellar planes of about 6 nm. Fig. 6(a) and (b) shows the micrographs of the catalyst TFA11/S15H, and it is observed that a part of the hexagonal pore structure remains under synthesis conditions (i.e., plane (100)), while other areas are rather damaged by triflic acid, which in turn promotes the formation of large pores and less ordered (left image) pore structures; this is reflected through the presence a less intense XRD peaks at 0.58° (2θ). Fig. 6(c) and (d) shows small particles of NiC/SBA-15 and MoC/SBA-16 respectively.

3.4. Physical adsorption of N₂

Table 1 exhibits the results on the textural properties of catalysts and supports. The characteristic properties of SBA-15 show a surface area of about 900 m²/g and average pore diameters

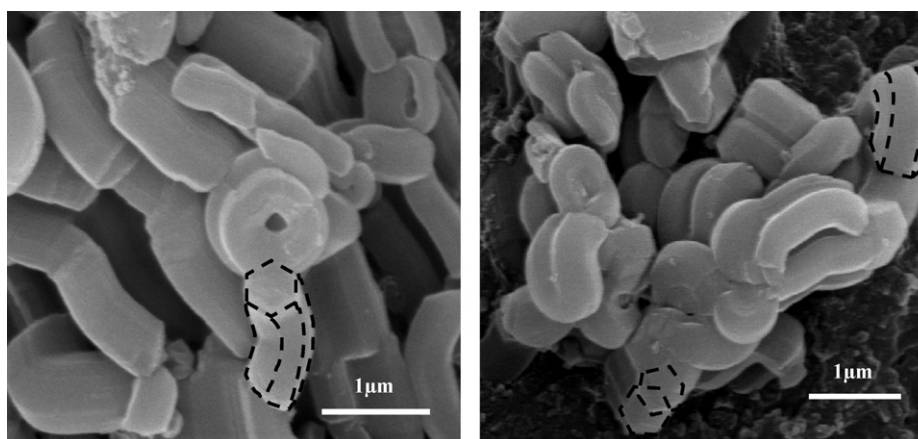


Fig. 4. SEM micrographs of the SBA-15 support. The typical morphology of the SBA-15 aggregates is evident, which is induced by the agitation pattern.

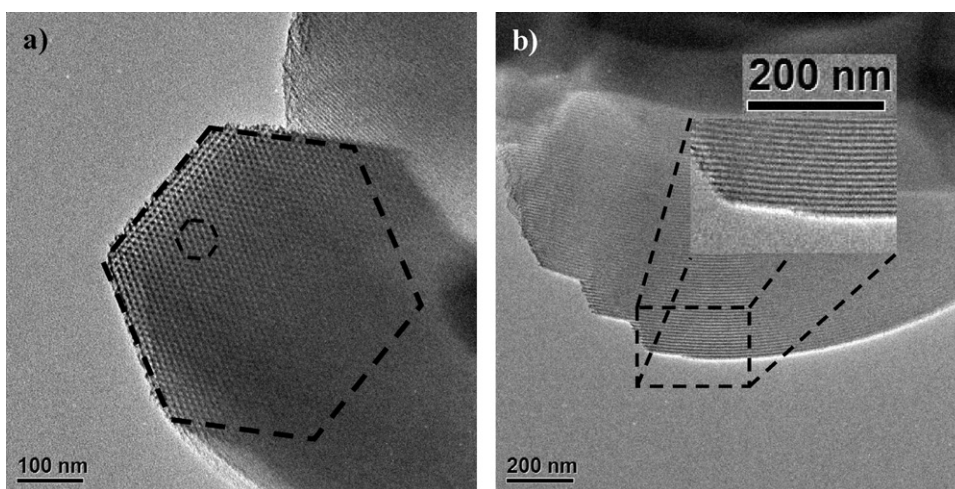


Fig. 5. TEM micrographs of the SBA-15 support. (a) The hexagonal arrays of pores are clearly observed on the tip of a small particle. (b) Side view of a SBA-15 particle.

and wall thickness of 4 nm and 8 nm, respectively. Most of the synthesized catalysts show a high surface area in the interval 600–800 m²/g, except NiMo and NiW carbides, which exhibit a substantial decrease of about 80%, and this is related to a loss of ordering in the porous materials (Fig. 3); Table 2 illustrates that about 2 to 5% of the total area of the materials count for the outer area, while over 90% is the inner surface area inside pores. Even in those cases the surface area is about 180 m²/g. For the series of catalysts Pt/SBA-15 the surface area is comparable with the SBA-15 support but their average pore diameter (up to 5.5 nm) is slightly higher as compared with the support (i.e., 4 nm). This is possibly produced by the pore space created within the cluster (C₅H₇O₂)₂, which is present in the platinum salt used in the catalyst synthesis. The incorporation of phosphorus in these catalysts provokes a slight decrease in the average pore diameter, together

with a slight increase in wall thickness. The TFA/SBA-15 catalysts showed a slight decrease in the total surface area and wall thickness after impregnation, with respect to the support alone, whereas, those impregnated with acetone showed extremely lower areas (about 50 m²/g) and destruction of the pore hexagonal symmetry. These results led us to conclude that catalysts TFA/SBA-15A were not adequate. Fig. 7 illustrates the typical isotherms showing adsorption–desorption curves corresponding to the support SBA-15. The curves are typical of a type IV isotherm with H1 hysteresis type, which corresponds to a mesoporous solid with cylindrical channels having a uniform shape and size, thus confirming the observations made by transmission electron microscopy (Fig. 5). Also, Fig. 8 presents the pore diameter distribution of the support, where a unimodal type distribution is predominant at about 5 nm.

Table 2
Structural and textural properties of catalytic materials.

Materials	d_{100} (nm)	a_0 (nm)	A_t (m ² /g)	A_n (m ² /g)	A_{ext} (m ² /g)	V_n (cc/g)	V_t (cc/g)	D_p (nm)	D_n (nm)	D_{BJH} (nm)	H_w (nm)
SBA-15	9.8	11.3	892.5	871.5	21.0	0.72	0.86	3.8	3.3	5.0	8.00
CNM/S15P	9.6	11.0	187.0	180.8	06.2	0.24	0.35	7.6	5.3	–	5.69
CNW/S15P	9.3	10.7	173.6	168.6	05.0	0.25	0.31	7.1	5.9	–	4.77
0.5Pt/S15	9.8	11.3	750.2	718.5	31.7	0.67	0.77	5.6	5.0	5.5	6.30
0.5Pt/S15P	–	–	558.0	538.9	19.1	0.66	0.79	4.1	3.8	5.0	–
1.0Pt/S15	10	11.5	819.5	782.3	37.2	0.73	0.84	5.7	5.1	6.5	6.40
1.0Pt/S15P	9.6	11.0	571.3	550.6	20.7	0.70	0.81	4.1	3.8	5.2	7.20
ATF7/S15	–	–	709.3	692.5	16.8	0.62	0.80	4.5	3.6	3.8/5.5	–
ATF11/S15	9.3	10.7	669.8	653.0	16.8	0.63	0.8	4.7	3.9	3.8/5.5	6.82

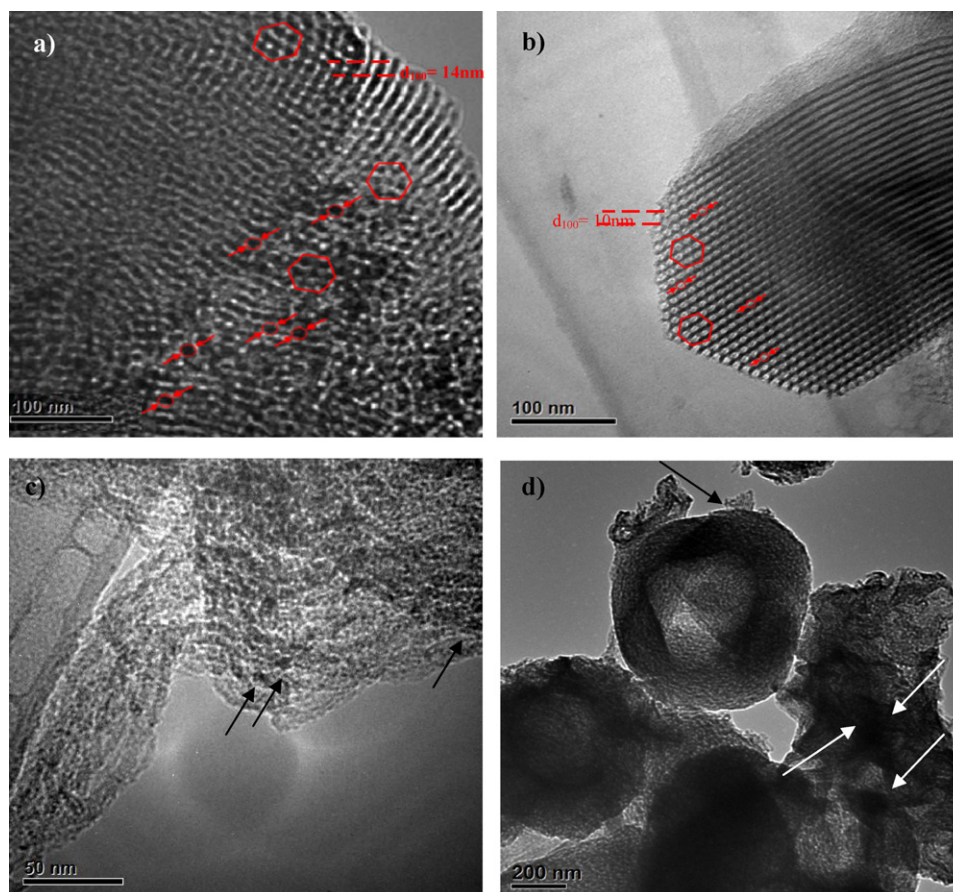


Fig. 6. Transmission electron micrograph of (a) and (b) TFA11/S15W. This material was synthesized under stirring using water solvent. (c) Nickel carbide particles on SBA-15 and (d) Molybdenum carbide supported on SBA-16.

3.5. Catalytic properties

The catalytic reactions were performed and compared with respect to an industrial catalyst based upon Ni–Mo/ γ -Al₂O₃ (i.e., commercial name: DSD3⁺). Fig. 9 clearly shows the distribution of products at different reaction temperatures using this catalyst; it is observed that at 623 K there is no significant increase in the prod-

ucts distribution but at higher temperatures there occurs a constant decrease of the heavy residues, which is mainly due to the generation of incondensable light gases; at this point it was decided to set the optimal reaction temperature at 613 K. Fig. 10 shows the evolution of the products distribution with time at constant temperature. As observed, after 180 min of reaction, no significant changes occur in the products distribution; for this reason it was decided to conduct all subsequent reactions at a setting time of 3 h and all the tests were conducted under these conditions. The reaction products were identified by prefixing the name of the HC catalyst used

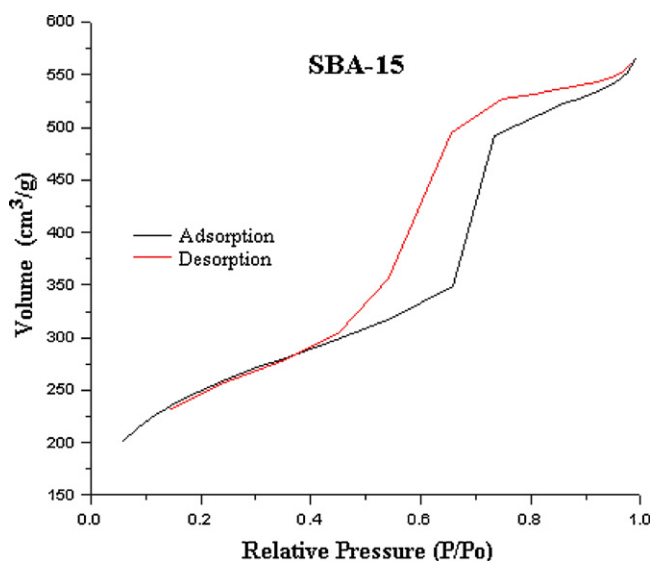


Fig. 7. N₂ adsorption-desorption isotherm at 77 K of SBA-15 support.

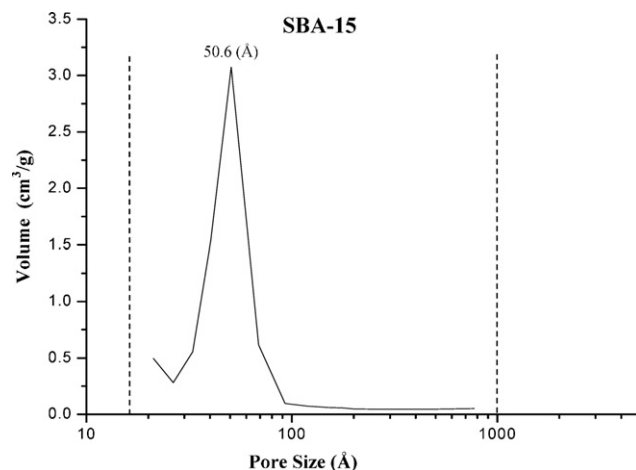


Fig. 8. Pore size distribution of the SBA-15 catalyst support.

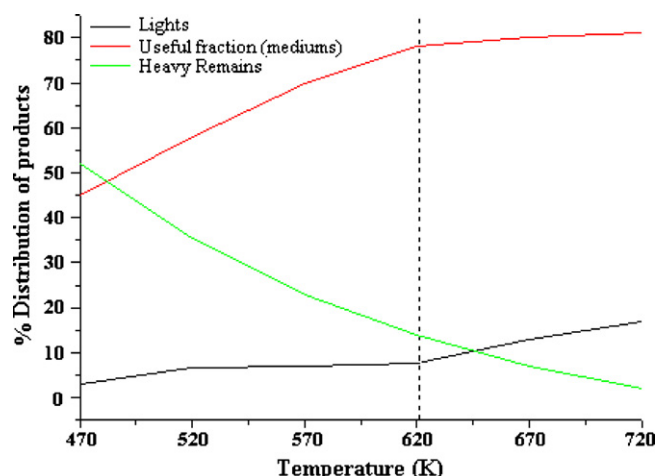


Fig. 9. Distribution of hydrocracking products obtained from green oil at different reaction temperatures, using a commercial catalyst, i.e. (NiMo/γ-Al₂O₃ (DSD3⁺)).

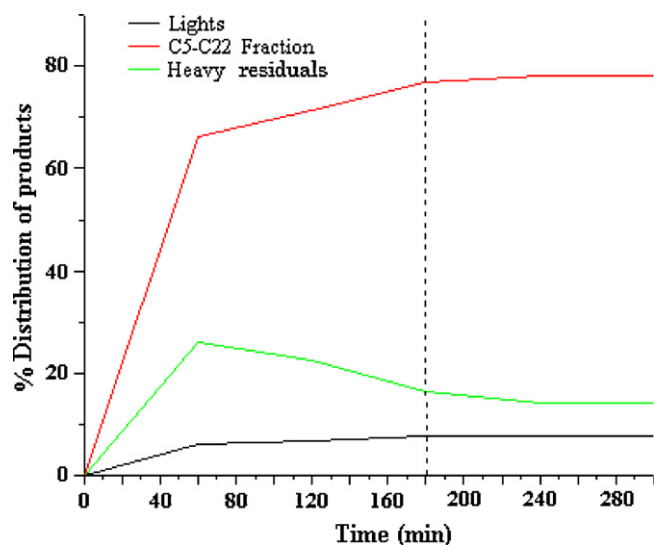


Fig. 10. Evolution of the principal product distribution for hydrocracking of green oil at 623 K, using a commercial catalyst (NiMo/γ-Al₂O₃ (DSD3⁺)).

in each reaction, and the hydrocarbons fractions were identified and were defined as: lights (C1–C4), naphtha (C5–C9), kerosene (C10–C14), gasoil (C15–C23) and heavy residue (>C24), according to the nomenclature reported by Chow [21].

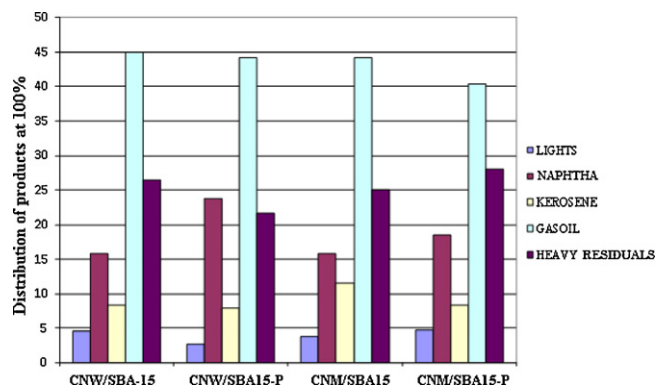


Fig. 11. Product distribution of the principal hydrocarbon fractions obtained from the hydrocracking on bimetallic carbides.

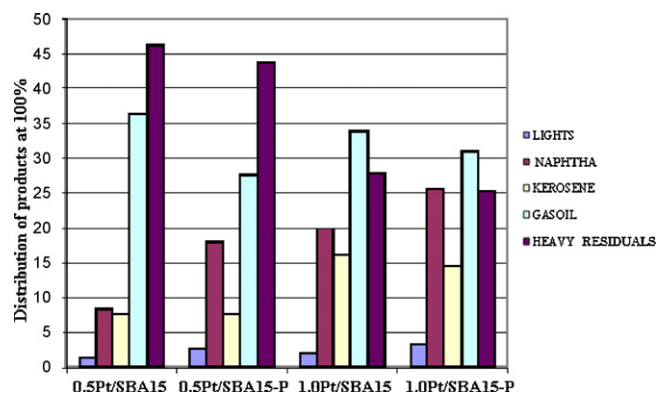


Fig. 12. Distribution of principal hydrocarbon fractions from the hydrocracking reaction using platinum catalysts.

Fig. 11 shows the hydrocarbons products distribution, which is normalized to 100%; in general the differences in the products distribution exist but are not exceptional when carbides type catalysts are used; however, the phosphorus-doped catalysts showed a conversion to naphtha fraction higher than their counterparts without phosphorus. The products obtained with the CNW/S15-P catalysts showed a (naphtha)/(heavy residue) ratio greater than 1, whereas others showed a ratio of less than 1. Fig. 12 shows the normalized distribution of hydrocarbons products that were obtained with platinum catalysts (series Pt/S15), which exhibited a low activity for the formation of light products (i.e., 0.5Pt/S15 and 0.5Pt/S15-P catalysts), while the selectivity to naphtha was similar than bimetallic carbides, except that there is a marked increase of the selective formation to kerosene and reduced diesel. The best catalyst for this series is 1Pt/S15-P, which showed a higher naphtha/(heavy residue) ratio as compared to other platinum catalysts. The catalysts impregnated with aqueous solutions of "triflic acid (TFA/S15H series) showed a slight increase towards the production of naphtha and a marked reduction of heavy residuum fraction, but the amount of light hydrocarbons was increased by 5%, reaching values close to 20% (see Fig. 13). The TFA11/S15H catalytic materials showed a higher conversion towards the production of naphtha. The best catalysts for each series were compared with industrial catalysts under the same operating conditions. Also, a reaction was performed without catalyst, in order to check the thermal effect on breaking C–C and C=C bonds. The results are displayed in Fig. 14, which shows that the heating effect is insufficient to break down heavier hydrocarbon molecules, thus generating a large amount of diesel and heavy residue. The industrial catalyst showed a lower production of heavy residues as compared with platinum catalysts and bimetallic carbides; its selectivity was oriented towards the formation of diesel while naphtha production barely exceeds 10%.

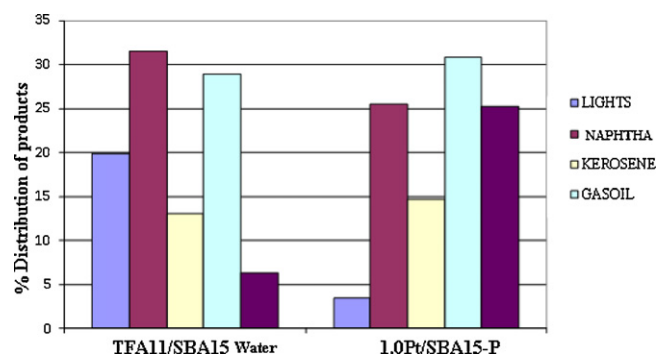
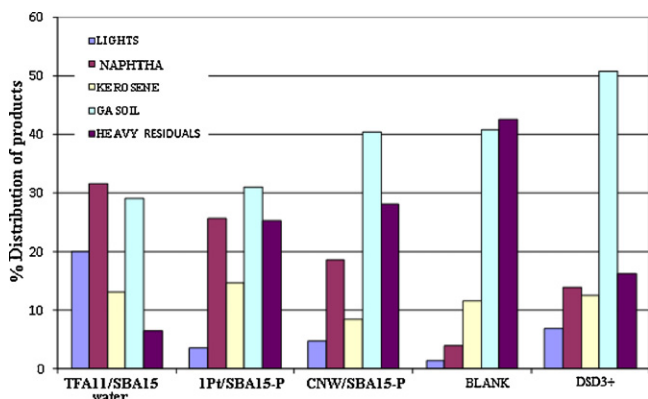


Fig. 13. Distribution of principal hydrocarbon fractions from the hydrocracking reaction using catalysts impregnated with triflic acid.

Table 3

Fatty acid content in vegetable oil and hydrocracking products.

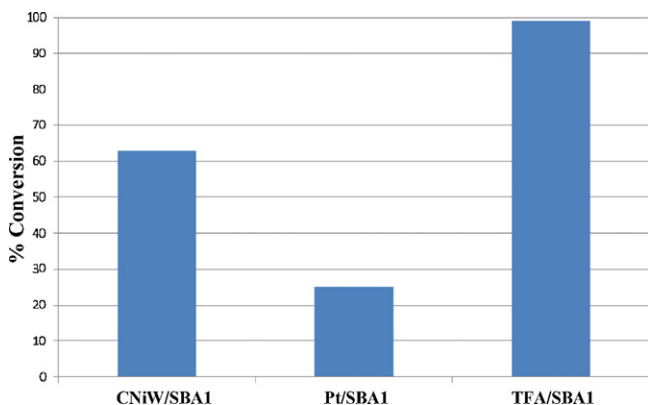
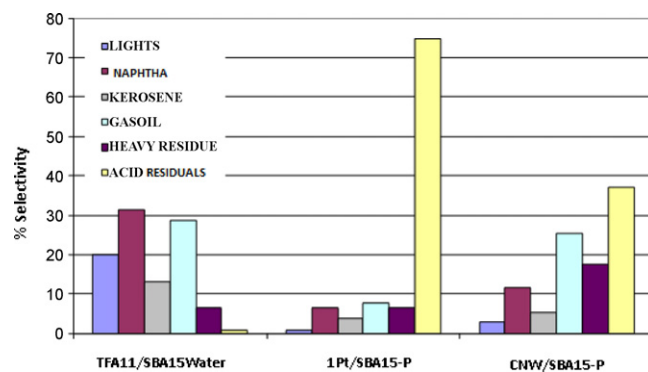
Compounds	Reactant AV-CAO		Product HC–CNiW/S15		Product HC–Pt/S15		Product HC–TFA11/S15	
	(mg)	wt.%	(mg)	wt.%	(mg)	wt.%	(mg)	wt.%
C16:0	0.51	6.34	0.61	20.47	1.2	19.93	N.D.	0
C18:2	0.66	8.20	0.07	2.35	0.38	6.31	N.D.	0
C18:1	6.63	82.36	1.82	61.07	3.57	59.30	N.D.	0
C18:0	0.2	2.48	0.43	14.43	0.76	12.62	0.07	100
C20:1	0.03	0.37	0	0.00	0.01	0.17	N.D.	0
C20:0	0.02	0.25	0.05	1.68	0.1	1.66	N.D.	0
Total	8.05	100.00	2.98	100.00	6.02	100.00	0.07	100

**Fig. 14.** Selectivity comparison of the best catalysts for hydrocracking of green oil ($T=623\text{ K}$, $t=3\text{ h}$ reaction time).

These results contrast with those obtained with the synthesized catalysts, where the conversions are close to 20% for the production of the fraction C5–C10.

A catalyst was used for the conversion of fatty acids to hydrocarbons but there was a better selectivity towards the naphtha and kerosene fractions. There are only few differences in the catalysts selectivity belonging to the same series, thus suggesting that their total conversion can be considered as very similar. Table 3 reports the content of fatty acids within three reaction products (i.e., HC–CNW/S15-P, HC–1.0Pt/S15-P and TFA11/S15H) and within the initial reactant (AV-CAO), while Fig. 15 shows the conversion for each reaction, which was calculated from the amount of fatty acids remaining in each product, as compared to the amount of fatty acids present in the initial reactant.

Fig. 16 shows the total distribution of products in the reactions performed with the use of nonmetallic TFA11/S15P, CNW/S15P and 1.0Pt/S15P. The selectivity reported in Fig. 16 was calculated after the total conversion and products distribution, using hydrocarbon

**Fig. 15.** Conversion percentage for hydrocracking reaction of green oil on the best catalysts at 613 K.**Fig. 16.** Selectivity for the best catalysts series.**Table 4**

Physical properties of the reaction products.

Sample	Specific gravity (d_4^{20})	$^{\circ}\text{API}$	Viscosity (cp)
HC–0.5Pt/S15	0.9220	21.3	469
HC–0.5Pt/S15P	0.9196	21.7	269
HC–1.0Pt/S15	0.9143	22.6	219
HC–1.0Pt/S15P	0.9114	23.1	193
HC–CNM/S15	0.9202	21.6	375
HC–CNM/S15P	0.9196	21.7	263
HC–CNW	0.9178	22.0	261
HC–CNW/S15P	0.9155	22.4	207
HC–TFA7/S15H	0.9016	24.8	34
HC–TFA11/S15H	0.8965	25.6	24
Light oil ⁽¹⁰²⁾	0.8409	36.0	8
Medium oil ⁽¹⁰²⁾	0.9019	24.7	73
Heavy oil ⁽¹⁰²⁾	0.9632	14.8	859
Diesel	–	–	3.16
Gasoline	–	–	0.18

standards, which allowed a more precise evaluation of the selectivity for each catalyst leading to the naphtha fraction. Clearly, the triflic acid catalyst showed the best performance towards the fraction C5–C10 (more than 30%), while the platinum supported catalyst had a very low yield, no larger than 10 wt.% with respect to the total products yield.

Also, Table 4 reports some of the most important physical properties of the reaction products, for different types of oil and commercial fuels. The values of density and viscosity for the reaction products are consistent with the composition of the samples. For example, the API gravity of most of the reaction products was very close to 22.3° API, which corresponds to the boundary between a medium and heavy crude. Only samples of the series HC–TFA/S15H have a viscosity and density corresponding to average crudes and this is consistent with the compositional analysis.

4. Discussion and conclusions

A dozen of SBA-15 supported catalysts were synthesized and were classified into three series according to the supported active

phase: (1) Bimetallic Carbides (i.e., Ni–Mo and Ni–W), (2) trifluoromethanesulfonic (triflic) acid, which was impregnated into the support from aqueous solutions and acetone and (3) Platinum. The structural properties of both, support and catalysts, were characterized by X-ray diffraction and transmission electron microscopy, while the textural properties were determined by N_2 physical adsorption (BET's method). The main XRD peaks of the SBA-15 support were verified at low Bragg angles, i.e., corresponding to (100), (110) and (200) planes, which are compatible with the hexagonal symmetry of the pore arrays. After impregnation structural modifications of the porous structure occur but the supported platinum and the triflic acid catalysts prepared from aqueous solutions retained the SBA-15 porous structure; in contrast, the pore hexagonal arrays of catalysts impregnated with triflic acid in acetone solution collapsed, as well as those corresponding to bimetallic carbide catalysts, i.e., the XRD peaks at 0.9° , 1.6° and 1.8° (2) are absent. The surface area of the SBA-15 support was about $900\text{ m}^2/\text{g}$; after impregnation of the catalytic active phases the surface area decreases down to about 200 and in some cases $700\text{ m}^2/\text{g}$. Only TFA/S15A type catalysts (triflic acid impregnated on SBA-15 in acetone solution) showed areas too low to work with. In general, the average pore diameters of the support and supported catalysts showed values between 4 and 7 nm, which falls into the range of mesopores. The transmission electron micrographs confirmed the XRD and N_2 physical adsorption data. The TFA11/S15H catalyst showed pore diameters and a basal spacing larger than original support, which is probably due to the abrasive effect of triflic acid. The destruction of the pore system is expressed on the XRD patterns as widening of the original peaks, peak shifts towards the lower Bragg angles and appearance of new peaks, which indicates that bigger pores might result from coalescence of smaller pores. The FTIR and non-diffuse reflectance studies showed the presence of Lewis type acid sites in the platinum (1.0%) and Ni–W carbide catalysts doped with phosphorus. Only catalysts impregnated with triflic acid in aqueous solution presented Bronsted type acid sites. The reaction temperature at 613 K was chosen in function of the nature of chemical species in the reaction mixture; comparatively, commercial catalysts are effective above 673 K for the hydrocracking reaction and some modeling works with medium size linear paraffins, i.e., n-heptane, have used lower hydrocracking temperatures, down to about 490 K [22,23]. Also, one observes that the catalysts with a low surface area (i.e., both industrial and bimetallic carbide catalysts) show a greater selectivity towards the formation of diesel and mid-cut products. The catalysts of the series TFA/S15H showed a greater selectivity towards the formation of naphtha (>30%), while the HC–CNIW/S15 and HC–Pt/S15 catalysts showed higher selectivity towards gasoil and a lower conversion of fatty acids into hydrocarbons, with residuals of fatty acids ranging from 30 to 70%. The viscosity and API gravity of the reaction products was measured and compared with medium and heavy crude oil, commercial diesel and gasoline. Most of the reaction products showed properties closer to heavy crude but the series of products obtained with the HC–TFA/S15H catalysts presented some characteristics of average crude. This catalyst showed a selective behavior towards medium size chain hydrocarbons, i.e., C18:0, while the HC–CNIW/S15 and HC–Pt/S15 catalysts were more selective towards the C18:1 type products. The distinct nature of the catalysts emphasizes the mono- and bifunctional catalysts character, i.e., HC–CNIW/S15 and HC–Pt/S15 are expected to promote hydrogenation–dehydrogenation reactions on the “metal” type sites while cracking of the olefin intermediaries is expected

to occur on the acid sites via a carbenium ion mechanism. However, the HC–TFA/S15H catalysts should act only via acid sites, without previous dehydrogenation leading to olefins, as no metal sites are present. It was reported previously that pure acid sites may generate carbenium ions from olefin by proton transfer, then this carbenium ion cracks and it is hydrogenated afterwards. The question is how the HC–TFA/S15H catalysts act in hydrocracking type reactions when no metal phase is present. The cracking of linear paraffins has been studied extensively and it has been verified that the rate of cracking increases with molecular chain length and one possible initiation step is carried out on Lewis type sites [24,25], which might promote carbenium ions formation by hydride abstraction from the paraffin [26,27]. Another possible initiation mechanism that is energetically more favorable involves the proton insertion to form penta-coordinated carbonium ions that crack similarly to carbenium ions [28,29]. Initial ions formed from olefins and paraffins are not the same, even if a carbenium ion is formed in both cases, i.e., the ion of olefins is formed on a Bronsted site (proton insertion) while ions formed from paraffins require a Lewis type site (hydride abstraction). Previous works [30] on HZSM5 type zeolites have led to conclude that the initiation proceeds either via a carbonium ion formed on a Bronsted site or a carbenium ion formed on a Lewis type site. For the present case, the product distribution obtained with catalysts having a “metallic” character, i.e., HC–CNIW/S15 and HC–Pt/S15, is different to the one obtained with acidic catalysts without metal phases, i.e., HC–TFA/S15H. The selectivity of the formers tends to favor gasoil formation and heavy residues (Fig. 14), while the selectivity of the non-metallic catalysts tends to form naphtha products preferentially, with no heavy residuals.

References

- [1] I. Sami Nashawi, *Energy & Fuels* 24 (2010) 1788–1800.
- [2] The Cancun Climate Summit, Mexico, <http://www.global-energy.org/international/cancun-climate-summit/conference-news> (December 2010).
- [3] J.H. Gary, G.E. Handwerk, *Petroleum Refining, Technology and Economics*, second ed., Marcel Dekker, Inc., New York, 1994.
- [4] I. Kubickova, D. Kubicka, *Waste Biomass Valor* 1 (2010) 293–308.
- [5] S. Ooi, R. Zakaria, A.R. Mohamed, S. Bhatia, *Catal. Lett.* 84 (2005) 295–302.
- [6] W. Charusiri, T. Vitidsant, *Energy Fuels* 19 (2005) 1783–1789.
- [7] M. Ternan, *Energy Fuels* 12 (1998) 239–247.
- [8] B. Egia, J.F. Cambra, P.L. Arias, *Appl. Catal. A* 169 (1998) 37–53.
- [9] A.I. Reyes de la Torre, J.M. Domínguez, J.A. Melo-Banda, C.E. Ramos, G. Sandoval, R.C. Angeles, M.R. Torres, *Catal. Today* 148 (1–2) (2009) 55–62.
- [10] A. Barbosa, B. Carlota, M. Pais, *Catal. Today* 98 (2004) 109.
- [11] R. Galiasso, L. Caprioli, *Catal. Today* 109 (2005) 185.
- [12] Z. Shuangqin, B. Juliette, *Appl. Catal. A* 294 (2005) 59–67.
- [13] J.C. Yori, J.M. Grau, V.M. Benitez, *Catal. Lett.* 67 (2005) 100.
- [14] O.P. Strausz, W. Thomas, *Energy Fuels* 13 (1999) 558–569.
- [15] T. Yamada, H. Zhou, *Mater. Lett.* 56 (2002) 93–96.
- [16] D. Zhao, J. Sun, Q. Li, G.D. Stucky, *Chem. Mater.* 12 (2000) 275.
- [17] L. Volpe, M. Boudart, *J. Sol. State Chem.* 59 (1985) 332–347.
- [18] L.A. Santillan-Vallejo, J.A. Melo-Banda, J.M. Domínguez, J.A. De los Reyes-Heredia, *Catal. Today* 109 (2005) 33–41.
- [19] Y. Park, T. Kang, J. Lee, P. Kim, H. Kim, J. Yi, *Catal. Today* 97 (2004) 195–203.
- [20] Ramos Galván C.E. Ph.D. Thesis, ITCM, Mexico, 2000, pp. 22–25.
- [21] S.P. Chow, *Petroleo y Sociedad*, FCE, Mexico, 1989.
- [22] K.I. Alhumaizi, V.M. Akhmedov, S.M. Al-Zahrani, S.H. Al-Khowaiter, *Appl. Catal. A: Gen.* 219 (2001) 131–140.
- [23] B.W. Wojciechowski, *Rev. Chem. Intermediat.* 8 (1987) 21–51.
- [24] M.R. Basila, T.R. Kantner, *J. Phys. Chem.* 70 (1966) 1681.
- [25] J.A. Schwarz, B.G. Russell, H.F. Haxnberger, *J. Catal.* 54 (1978) 3033.
- [26] D.M. Nace, *Ind. Eng. Chem. (PRD)* 8 (1969) 31.
- [27] A. Borodziński, A. Corma, B.W. Wojciechowski, *Can. J. Chem. Eng.* 58 (1980) 219.
- [28] G.A. Olah, Y.K. Mo, J.A. Olah, *J. Am. Chem. Soc.* 95 (1973) 4939.
- [29] G.A. Olah, J.R. De Member, J. Shen, *J. Am. Chem. Soc.* 95 (1973) 4952.
- [30] J. Abbot, B.W. Wojciechowski, *Ind. Eng. Chem.* 24 (1985) 501.